



Article

Seasonal Variation in Land and Sea Surface Backscatter Coefficients at High Frequencies

Danielle Edwards and Manuel Cervera



<https://doi.org/10.3390/rs14215514>



Article

Seasonal Variation in Land and Sea Surface Backscatter Coefficients at High Frequencies

Danielle Edwards ^{1,*} and Manuel Cervera ^{1,2} ¹ Defence Science and Technology Group, Edinburgh 5111, Australia² School of Physical Sciences, The University of Adelaide, Adelaide 5005, Australia

* Correspondence: danielle.edwards@defence.gov.au

Abstract: Over the horizon radars (OTHR) rely on the propagation of high frequency (HF) radio waves via the ionosphere to successfully achieve their designated missions. Backscatter sounders (BSS) are environmental over-the-horizon radars which may be used to assess the ionospheric propagation conditions. However, high power observed by a BSS may be due to either good ionospheric propagation, a high surface backscatter coefficient, or a combination of both. Hence, an understanding of the surface backscatter coefficients and their temporal variation is essential to fully understand the ionospheric propagation conditions. A database of surface backscatter coefficients over a decade was created using backscatter ionogram data from four backscatter sounders in Australia. The temporal variations in the backscatter coefficients were investigated and it was found that the land backscatter coefficients were relatively constant over time, while the sea backscatter coefficients showed significant seasonal variation.

Keywords: over-the-horizon radar; backscatter coefficient; high frequency radar; seasonal variations



Citation: Edwards, D.; Cervera, M. Seasonal Variation in Land and Sea Surface Backscatter Coefficients at High Frequencies. *Remote Sens.* **2022**, *14*, 5514. <https://doi.org/10.3390/rs14215514>

Academic Editor: Kun-Shan Chen

Received: 19 September 2022

Accepted: 1 November 2022

Published: 2 November 2022

Publisher's Note: MDPI stays neutral with regard to jurisdictional claims in published maps and institutional affiliations.



Copyright: © 2022 by the authors. Licensee MDPI, Basel, Switzerland. This article is an open access article distributed under the terms and conditions of the Creative Commons Attribution (CC BY) license (<https://creativecommons.org/licenses/by/4.0/>).

1. Introduction

Knowledge of the surface backscatter coefficient of radio waves in the high frequency (HF) band is important for understanding the ionospheric propagation conditions for over-the-horizon radar (OTHR) [1,2], and can be used for remote sensing of the surface [3]. The backscatter coefficient characterises the amount of radiation scattered back from a surface towards a receiver per unit area. This is dependent on the radio wave and surface properties, including the polarisation, angle of incidence and frequency of the scattered waves, and the surface roughness and conductivity [4]. Hence, as these surface properties change over time it is expected that the backscatter coefficient will too.

Extensive research has been conducted on how the backscatter coefficient is affected by the surface roughness [4,5] and surface features such as mountains, trees, and buildings [2,6–9]. This is of interest for use in the conversion of radar coordinates to geographic coordinates, known as coordinate registration [10,11]. The sea backscatter coefficient at HF has also been studied in detail due to interest in remote sensing of the sea state and surface targets [3,12–15].

Investigations into the seasonal variation in OTHR ground backscatter returns have been conducted [1,16]; however, these studies have focussed on seasonal variations in the ionospheric propagation conditions rather than the variations in the surface backscatter coefficients. Limited analysis has been performed on the seasonal variations in the backscatter coefficient at HF. Gardiner-Garden and Pincombe [17] investigated the seasonal patterns in the HF backscatter from the sea, and found there was significant seasonal and spatial variability. For parts of the Northern Australian region where light and variable winds dominate, considerable seasonal variability in the backscatter coefficient (approximately 20 dB) was found, while for parts of the Australian region where the winds are strong and steady the seasonal variability in the sea backscatter coefficients was as low as 3 dB.

This paper describes a long-term study of surface backscatter coefficients to investigate the seasonal variability. Section 2 describes the data and the method that were used to calculate the surface backscatter coefficients over a decade. Section 3 presents the results, and shows there is a prominent yearly cycle in the sea backscatter coefficients, while the land backscatter coefficients remain relatively constant over time. The results are also discussed in this section. The conclusions are summarised in Section 4.

2. Materials and Methods

Surface backscatter coefficients were calculated using a method of comparing observed backscatter ionograms with those modelled using radio-wave raytracing through an appropriate ionospheric model. For our purpose the ionospheric model must account for the day-to-day variability of the ionosphere. Climatological monthly median models of the ionosphere such as the International Reference Ionosphere (IRI) do not meet this requirement. Hence, to study the seasonal variation in the backscatter coefficient, a long term dataset of backscatter ionograms and a data conditioned ionospheric model were required.

2.1. Software and Data

2.1.1. Backscatter Ionograms

Backscatter ionograms from 2011 to 2020 were obtained from four backscatter sounders (BSS) at three locations in Australia: Longreach (LO), Queensland, Laverton East (LAE) and Laverton West (LAW), Western Australia and Alice Springs (AS), Northern Territory. These four BSS are part of the Jindalee Operational Radar Network (JORN) frequency management system (FMS). JORN is a network of OTHR operated by the Royal Australian Air Force (RAAF) to monitor the air–sea gap to the north of Australia [18,19]. Each of the JORN BSSs form eight beams within a 90 degree field of regard to produce eight backscatter ionograms. The location and field of view of the BSS data used in this study are shown in Figure 1. The group range resolution of this data was 50 km, the frequency resolution was 0.2 MHz and the power resolution was 0.5 dBW. The ionograms were scaled to a transmit power of 20 kW. A more detailed description of the BSS system and data is available in [2].

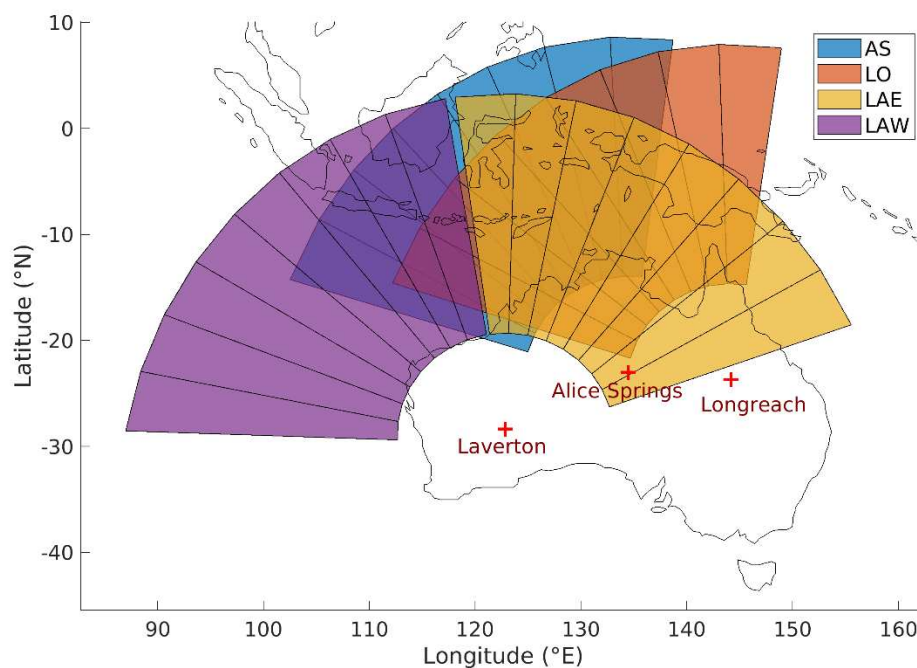


Figure 1. Fields of view of the four JORN FMS backscatter sounders. The inner and outer arcs are located at 1000 and 3500 km from the sounder.

2.1.2. Real Time Ionospheric Model

Real Time Ionospheric Model (RTIM) data from 2011 to 2020 were used for the modelling of backscatter ionograms. The RTIM is a data driven model, generated using data from the JORN FMS network of oblique and vertical incidence sounders [20,21]. The RTIM is built from quasi-parabolic layers that parametrise the electron density profile at all locations within the JORN field of view. A 3D grid of the ionospheric electron densities was obtained, and 2D slices were produced in the directions required for the ray tracing for modelling ionograms. The spatial resolution of this data is 1 degree in latitude and longitude and 1 km in height steps.

2.1.3. Raytracing Toolbox

The PHaRLAP raytracing toolbox was used for 2D numerical raytracing through the ionospheric model to produce synthetic backscatter ionograms. PHaRLAP is a MATLAB toolbox developed by Defence Science and Technology Group for modelling the propagation of high frequency radio waves through a model ionosphere [22]. The ray tracing algorithms account for many different propagation effects including geometric gains and losses via the focussing and defocussing of rays and ionospheric absorption.

2.2. Calculation of Surface Backscatter Coefficients

Surface backscatter coefficients were calculated using the method described in [2]. Backscatter ionograms were modelled using 2D numerical raytracing through a slice of the RTIM, where all losses other than the surface backscatter coefficient were included. Propagation losses such as focusing/defocusing and ionospheric absorption were accounted for. The George and Bradley climatological model of ionospheric absorption was used [23]. The transmit and receive antenna gains were modelled using a method-of-moments electromagnetic solver [24].

The difference in power between observed ionograms (Figure 2a) and the ionograms modelled for the same time and location (Figure 2b) was then found to obtain a measurement of the surface backscatter coefficient (Figure 2c). The shaded area in the top two panels in Figure 2 indicates the region of the ionogram deemed suitable for calculating the backscatter coefficient. The choice of this region is described in detail in [2]. Briefly, it is necessary to use that region of the ionogram which has only one ionospheric propagation mode contributing to it. That region is the 1-hop F2 lobe [2] beyond the leading edge.

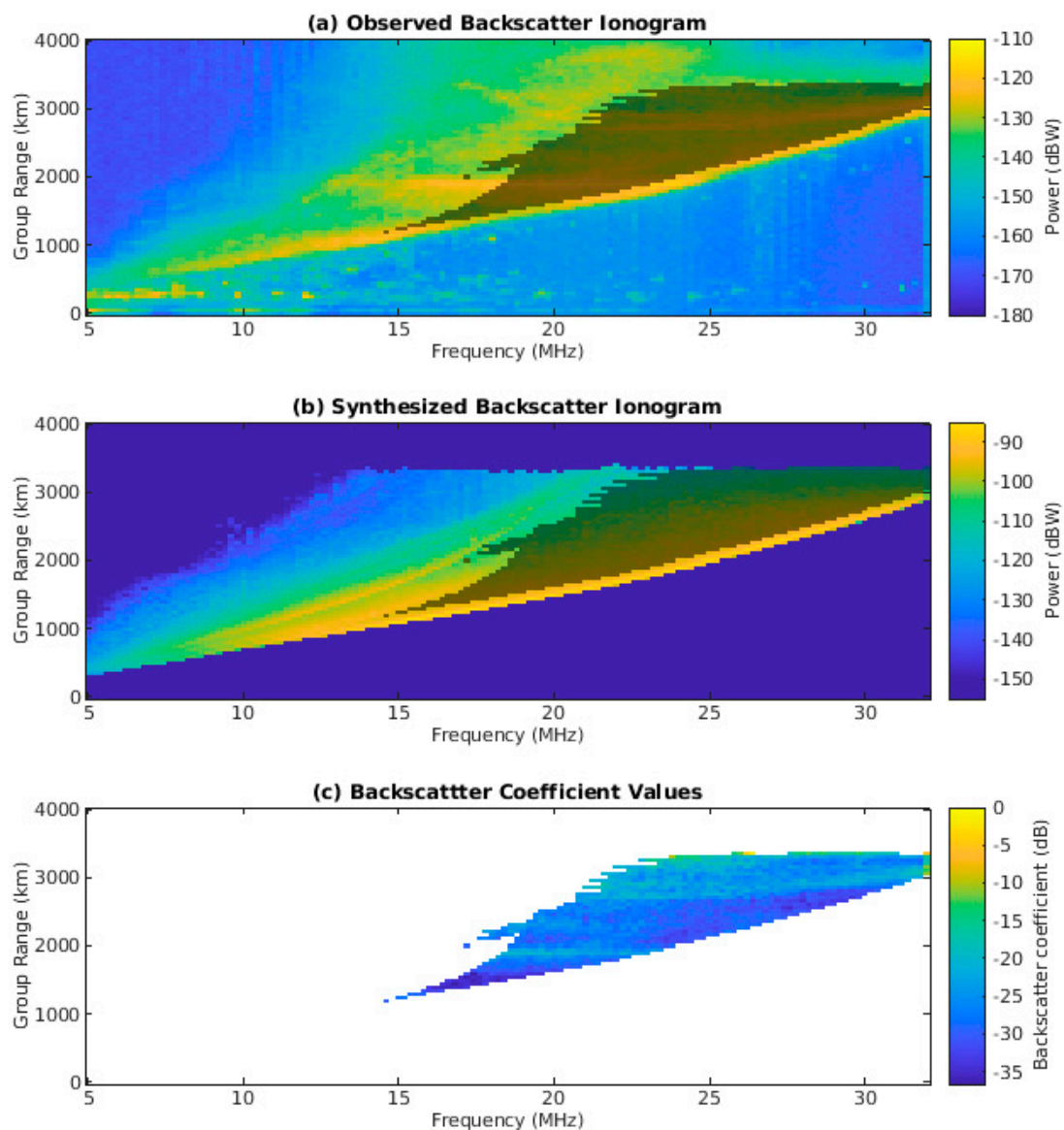


Figure 2. Observed (a) and modelled (b) backscatter ionograms with the area deemed suitable for calculating backscatter coefficients shadowed. Backscatter coefficient values (c) are obtained by taking the difference in power between the modelled and observed ionograms.

2.3. Investigating Seasonal Variation

It is expected that the backscatter coefficient will change over time as the surface conditions vary. A database of backscatter coefficients over a decade (approximately a solar cycle) was created to investigate the seasonal variation. A large number of model backscatter ionograms were required to be synthesized to build the database of the backscatter coefficients. Model backscatter ionograms were synthesized for each of the four backscatter sounders for all of their eight beams over a 10 year period. Due to the computational expense of modelling ionograms for all times that observed ionograms were available, only a selection of the days were used. Ionograms were only modelled for local day time hours as generally there are a larger number of frequencies available for ionospheric propagation during the day. For each month, ionograms were modelled for a selection of days (2, 6, 10, 14, 18, 22, 26 and 30) and times (1, 3, 5, 7 and 9 UT each day). Approximately 1000 to 1500 ionograms were modelled per month. Ionograms were modelled only for times when both the archived RTIM data and BSS ionograms were available.

The monthly mean backscatter coefficients were then calculated for each 50 km range cell for the 8 receive beams of the sounders to create maps of the backscatter coefficient in the same way as was done in [2]. An example of one of these maps is shown in Figure 3.

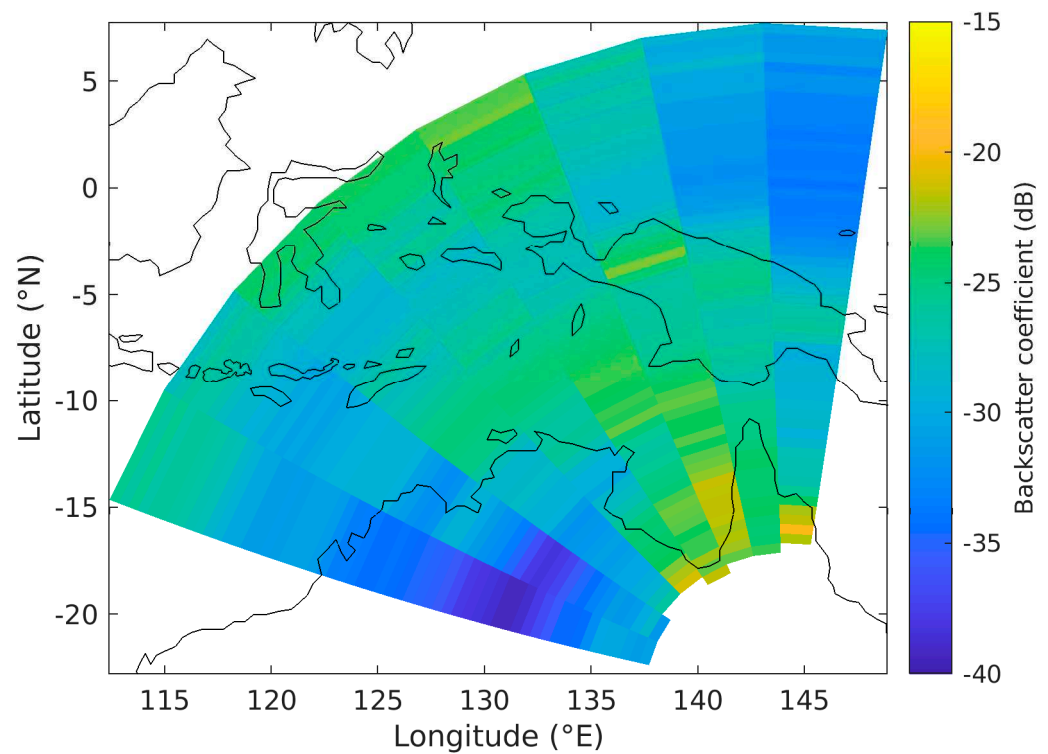


Figure 3. Map of the monthly mean backscatter coefficients for LO in January 2015.

3. Results and Discussion

3.1. Backscatter Coefficient Results over the Decade

The monthly mean backscatter coefficients were calculated over the decade for each of the four BSS. For brevity, only the LO results are shown for the monthly maps of the backscatter coefficient over the decade. However, the data reduction and detailed analysis are presented for all four sounders. Figures 4 and 5 show maps of the monthly mean backscatter coefficients for the LO sounder from January 2011 through to December 2020. Higher backscatter coefficients are more commonly seen in the middle of the year (from around June to August). Conversely, little variation is noted from year-to-year, indicating that while there is considerable seasonal variation, there is little variation over the 11 year solar cycle. The lack of variation over the solar cycle is expected as the solar cycle is a driver of the ionospheric propagation conditions and has little effect on terrestrial weather which is the main driver of the sea state. It is the variation of the sea state which affects the backscatter coefficient over the ocean.

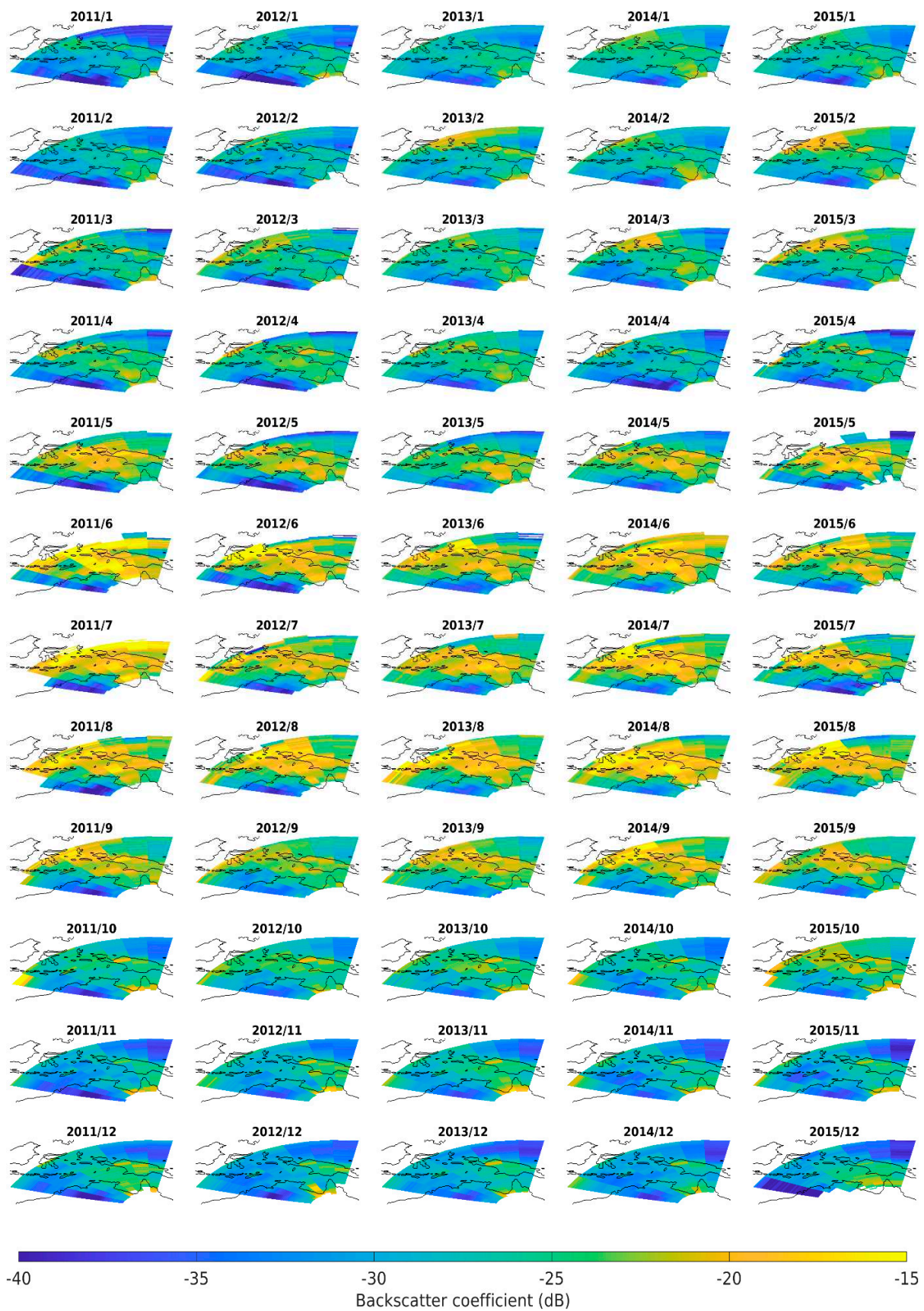


Figure 4. Monthly mean backscatter coefficients for LO over a 5 year period from January 2011 (top left plot) through to December 2015 (bottom right plot).

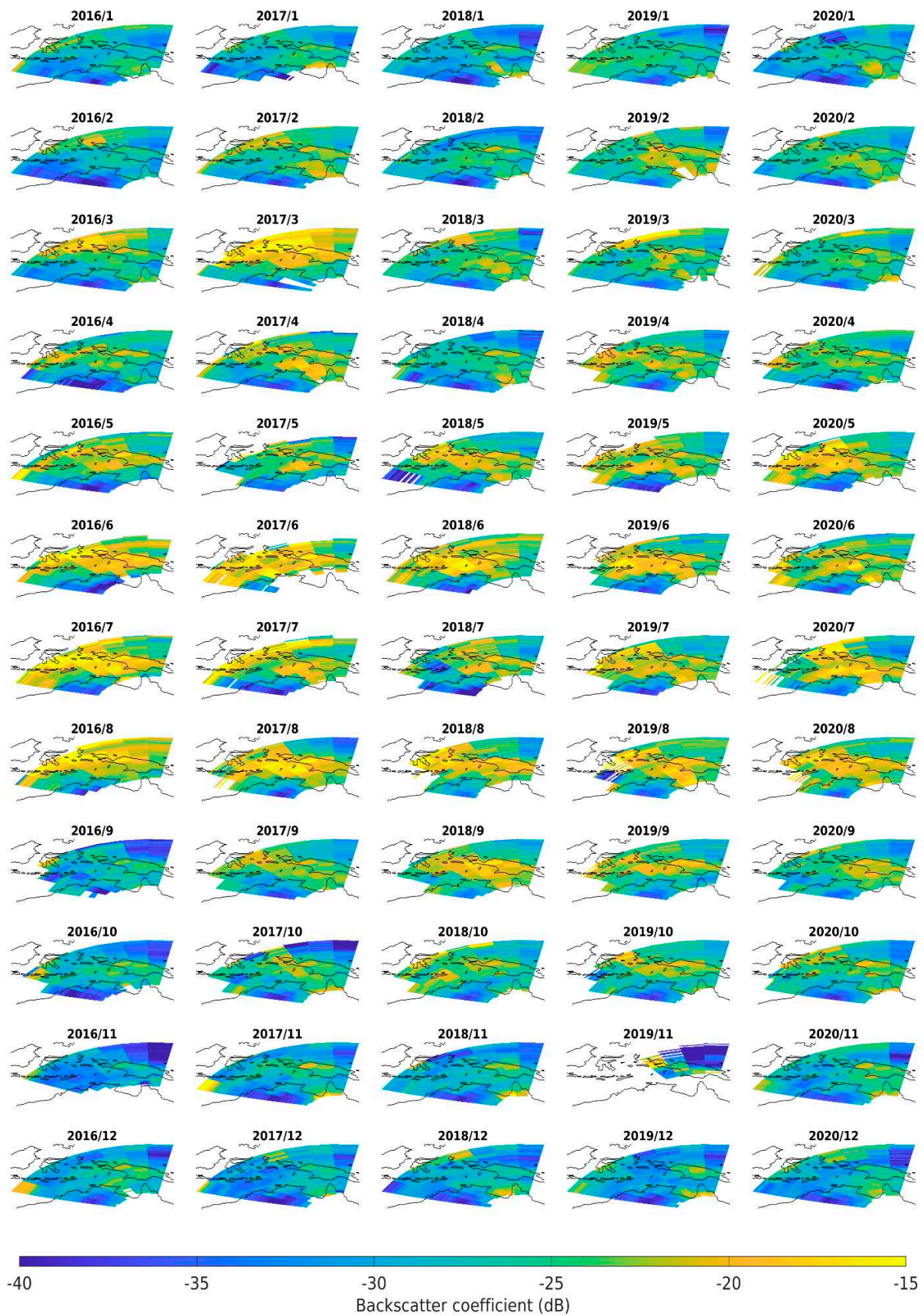


Figure 5. Monthly mean backscatter coefficients for LO over a 5 year period from January 2016 (top left plot) through to December 2020 (bottom right plot).

We can make an initial assessment of the difference between land and sea backscatter by examining the monthly standard deviation of the backscatter coefficients for each range azimuth cell calculated over the decade. Figure 6 shows the decade mean of the monthly standard deviation in the backscatter coefficients for each of the sounders. The standard deviation for LO was generally greater over the ocean (especially for the Arafura Sea (around 8°S, 136°E) and the Pacific Ocean (around 5°N, 135°E) where the mean standard deviation is as large as 9 dB). This suggests the sea backscatter coefficients change throughout each month more than the land backscatter coefficients, which is expected from changes in the sea conditions due to weather (as discussed in our earlier paper [15]). A range dependence in the standard deviation can be seen, which is attributed to limitations of the backscatter ionogram synthesis. Larger errors occur in the propagation model for longer distances. Consequently, the difference between the real and synthetic backscatter ionograms is potentially larger for longer distances (see our earlier paper [2]) which will lead to a larger random error in the calculation of the backscatter coefficient. This results in a larger standard deviation in the results at longer ranges.

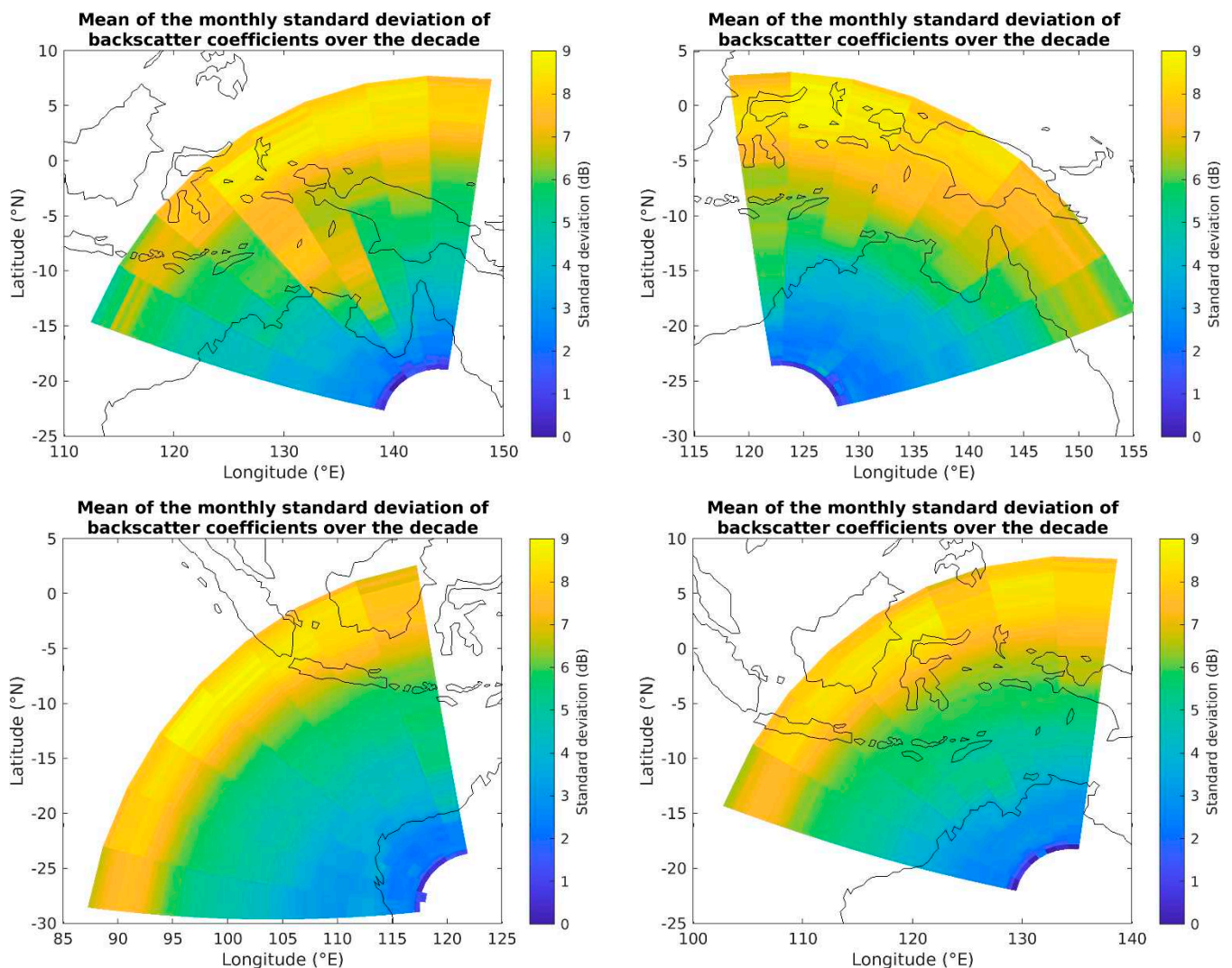


Figure 6. The decade mean of the standard deviation of each monthly value for LO (top left), LAE (top right), LAW (bottom left) and AS (bottom right).

The decade mean of the monthly mean backscatter coefficients for each of the sounders is shown in Figure 7. Various topographic features are visible in these maps of the backscatter coefficient. Of particular note is the strong backscatter from New Guinea (at around 5°S,

140°E) which is due to a large mountain range which runs centrally along the length of the island. This backscatter is stronger in the LAE sounder than LO which is due to the LAE sounder observing the mountain range orthogonally. In general, the lowest backscatter coefficients occurred over desert regions (such as at 20°S, 130°E and 23°S, 140°E), while the highest land backscatter coefficients occurred where the terrain was rough with mountainous features or highly vegetated (such as at 5°S, 140°E). We do not discuss this further here as land backscatter coefficients were investigated in detail in our earlier paper [2]. An aspect dependence can also be seen in the backscatter coefficients, where multiple sounders observe the same location from different directions (for example at 16°S, 130°E and at 5°S, 140°E).

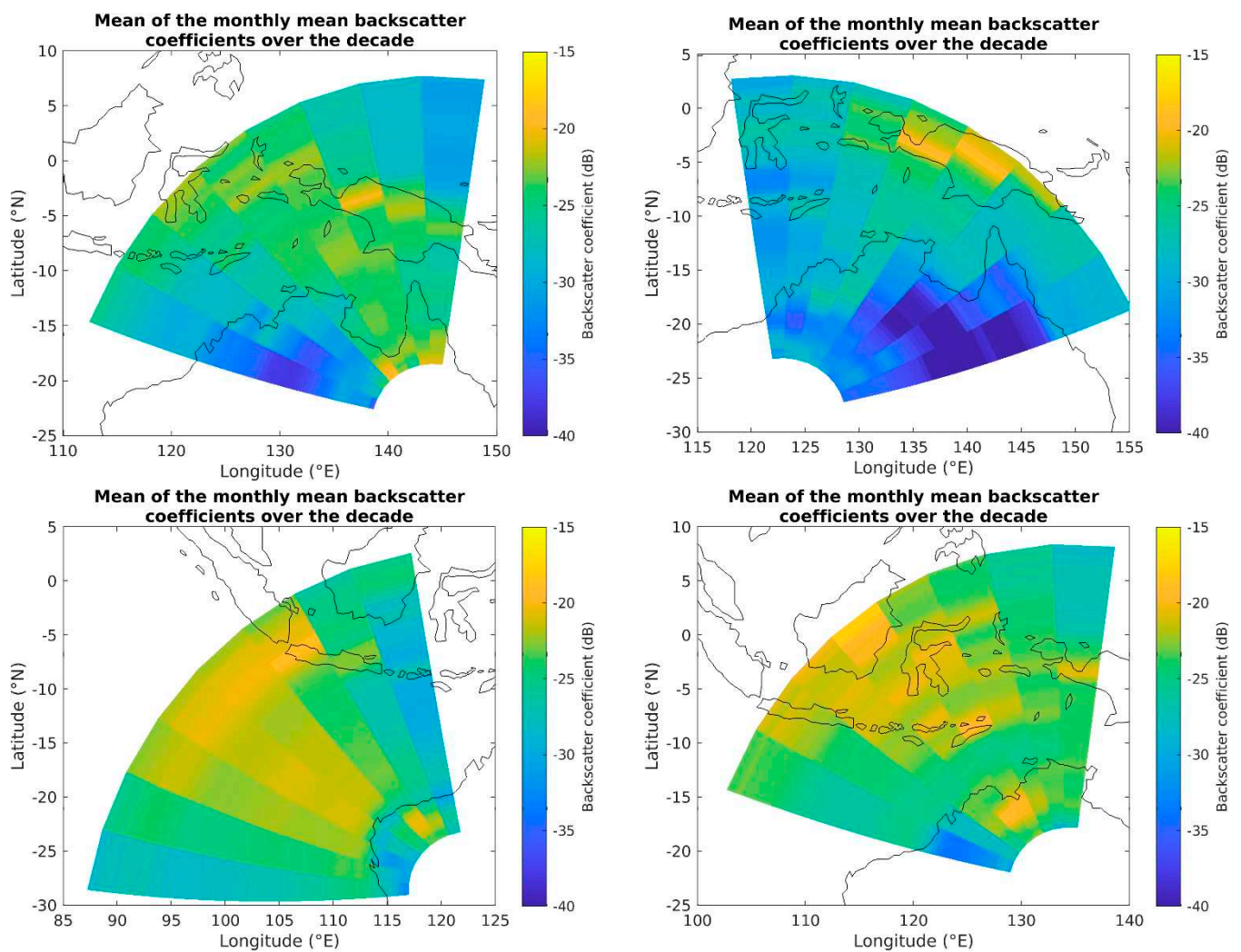


Figure 7. Decade mean of the monthly mean backscatter coefficients for LO (top left), LAE (top right), LAW (bottom left) and AS (bottom right).

Figure 8 shows the mean number of data points contributing to each range-azimuth cell each month. The maximum number of data points available occurred at ranges of 1500–3000 km as expected, as this is a common one hop range due to the ionospheric propagation support. This is important as areas with more data points have better statistics for the calculation of the surface backscatter coefficient, while the results for areas where few data points are available must be treated with caution as discussed later.

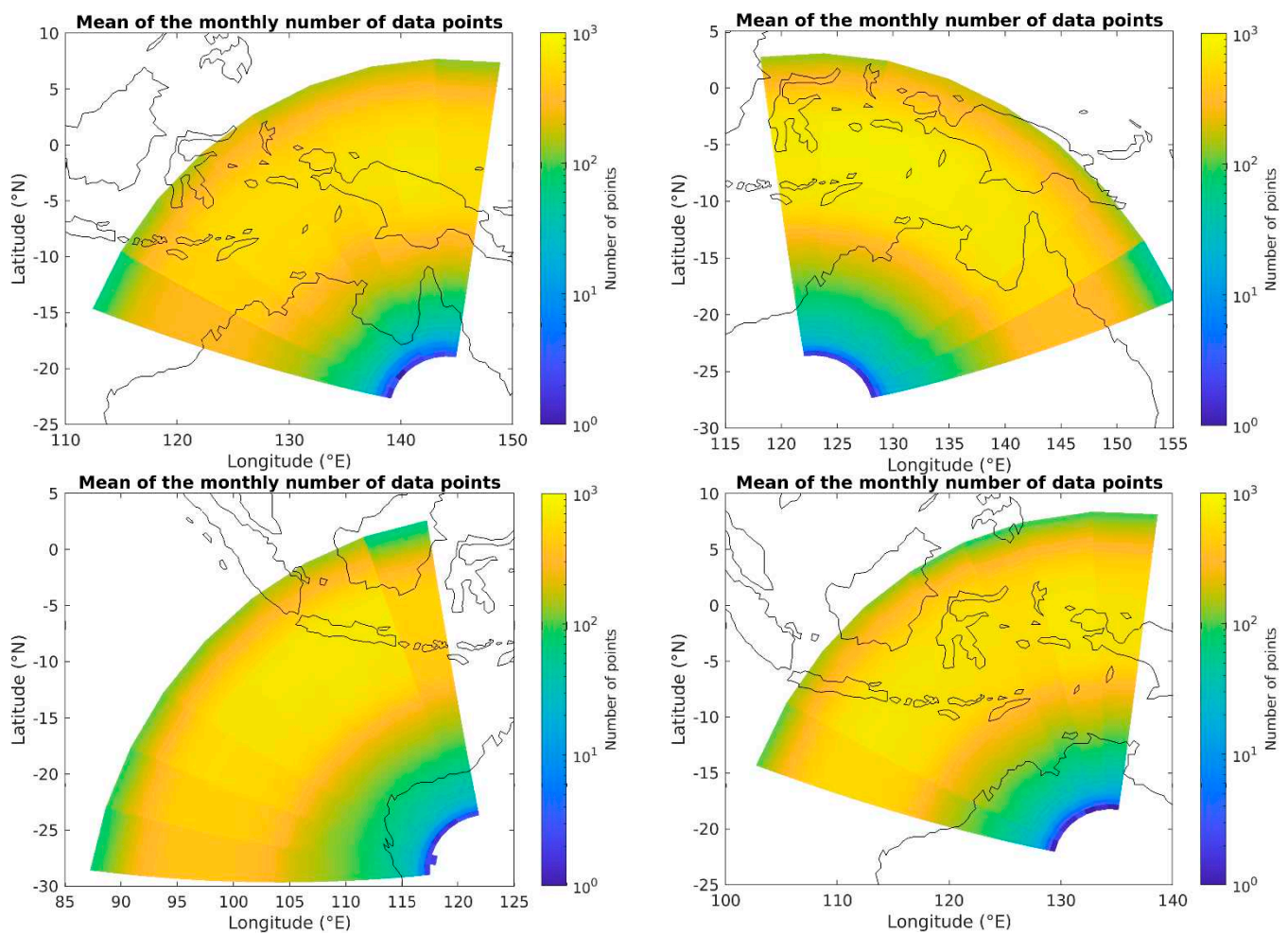


Figure 8. Decade mean number of data points contributing to each monthly backscatter coefficient value for LO (**top left**), LAE (**top right**), LAW (**bottom left**) and AS (**bottom right**).

3.2. Seasonal Variation in the Surface Backscatter Coefficients

To investigate the seasonal variation in the surface backscatter coefficients, the changes in the monthly mean backscatter coefficients for each location over time need to be examined. Before we can do this for the entire data set we first investigate the monthly backscatter coefficients at a single location: beam 4 of the LO sounder at a range of 3000 km (3°S , 127°E). This location was chosen as it exhibits a large standard deviation in the monthly mean backscatter coefficient over the decade of data. The entire time series of the monthly mean backscatter coefficient for this location is plotted in Figure 9 (left) and as a superposed epoch against the month of year in Figure 9 (right). The backscatter coefficient followed similar trends for all of the years. A clear trend of higher backscatter coefficients in the middle of the year can be seen. A Fourier transform was used to find the peak frequencies in this time series and the resultant amplitude spectrum is shown in Figure 10. No window was applied and missing data was filled with the mean value of the nearest data either side, weighted by their temporal offset to the missing data points.

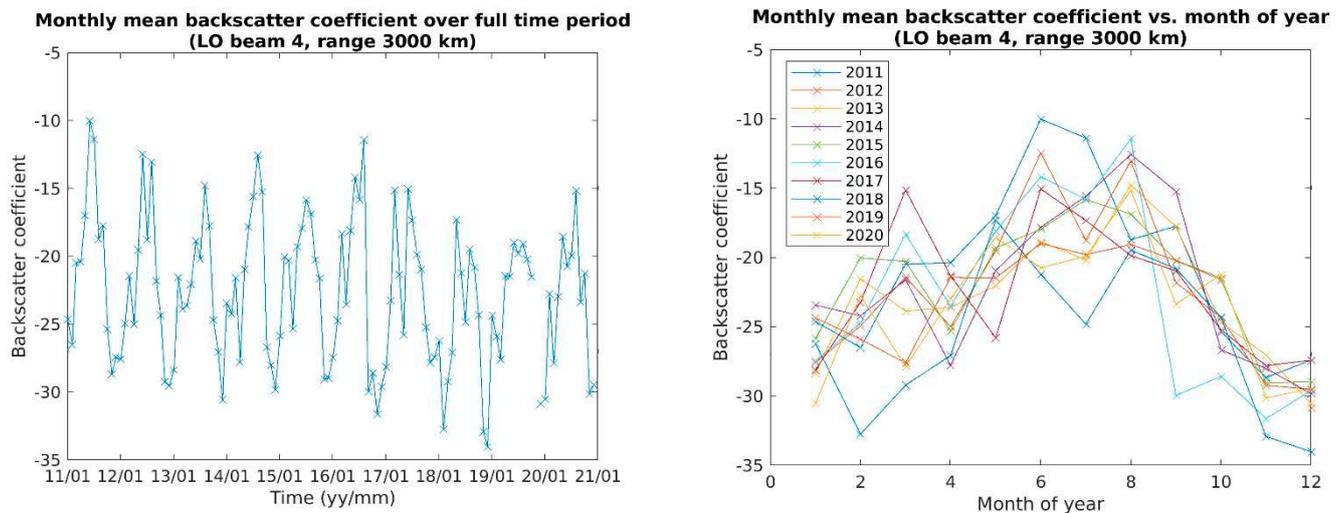


Figure 9. Monthly mean backscatter coefficient over time for LO beam 4, range 3000 km. (Left): plotted for the decade from 2011 to 2020. (Right): Plotted against the month of year.

Single-sided amplitude spectrum of the monthly backscatter coefficients over a decade (LO beam 4, range 3000 km)

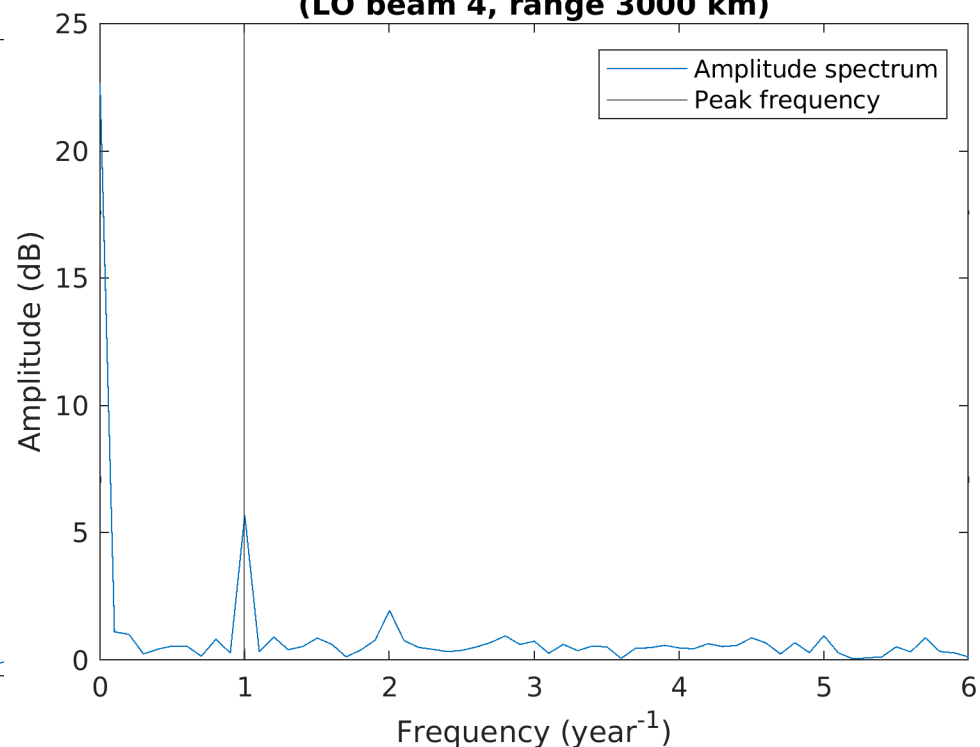


Figure 10. Single-sided amplitude spectrum from the FFT on the LO beam 4, range 3000 km data.

A clear peak in frequency at one cycle per year was found. A weaker biannual peak was also seen. This was not surprising as typically ocean wave heights follow a sinusoidal annual cycle with larger significant wave heights in winter due to seasonal changes in high latitude storm patterns [25]. Colosi, Villas Bôas and Gille [25] investigated the annual and biannual cycles in the significant wave height and wind speed globally. They showed there was a strong annual cycle in the wave height and wind speed in this location, and a weaker biannual cycle. It was suggested that the South Asian monsoon's biannual occurrence may

play a role in the biannual cycles in this region. The phase of the FFT indicates that the annual cycle peaks in July and the biannual cycle peaks in May and November.

The frequency and amplitude of the primary peak was calculated in the manner described above for each range azimuth cell of the LO data and plotted in Figure 11. Locations were not considered for this analysis if the monthly mean data availability was less than 50%. In the left panel, data with low statistical significance (see below) are not plotted. The primary-peak amplitude over the Australian landmass was, as expected, much less than over the sea. For most locations (considering both the land and sea) the peak frequency was one cycle per year. A peak frequency of two cycles per year was seen over Northern Australia; however, the amplitude of this peak was low, which shows there is little seasonal variation in this area. Figure 12 shows a histogram of the primary peak frequencies for the LO range-azimuth cells. This shows that a peak frequency of one cycle per year was the most common.

To determine the significance of the spectral peaks we employed a statistical technique described by [26]. Gaussian noise was generated with the same mean, standard deviation and number of data points as the monthly mean backscatter coefficients data for each range-azimuth cell. The fast Fourier transform was applied to this noise, and this was repeated for 1000 sets of noise. An amplitude threshold was then set at a level which is exceeded by less than 1% of the noise data. This amplitude threshold was then used to determine which peaks from the backscatter coefficient data were significant. Peaks in the Fourier amplitude spectrum were considered significant if the peak was greater than the amplitude threshold. The largest peaks in the Fourier amplitude spectrum for majority of the range-azimuth cells were considered significant.

This analysis shows that while the amplitude of the biannual peaks from the Northern Australian landmass is low, these peaks are statistically significant. We currently do not have an explanation for this variation as the rainfall and consequently changes to ground conductivity in this region has a strong annual variation peaking in late January. It is possible that seasonal variations in the ground properties at the backscatter sounder transmit and receive sites may affect the antenna patterns and thus the power transmitted/received, especially for low elevation rays. This could contribute to weak seasonal variations in the power of the backscatter ionograms that has not been accounted for by the model. Consequently, this could affect the backscatter coefficients, and may introduce the observed weak biannual cycle over land if the wet seasons at the transmit and receive sites and the observed locations are out of phase. However, the rainfall at Longreach, Queensland, is low and peaks in early February with a minimum in August, i.e., in phase with the observed locations and so we reject this hypothesis as an explanation of the observed weak biannual variation.

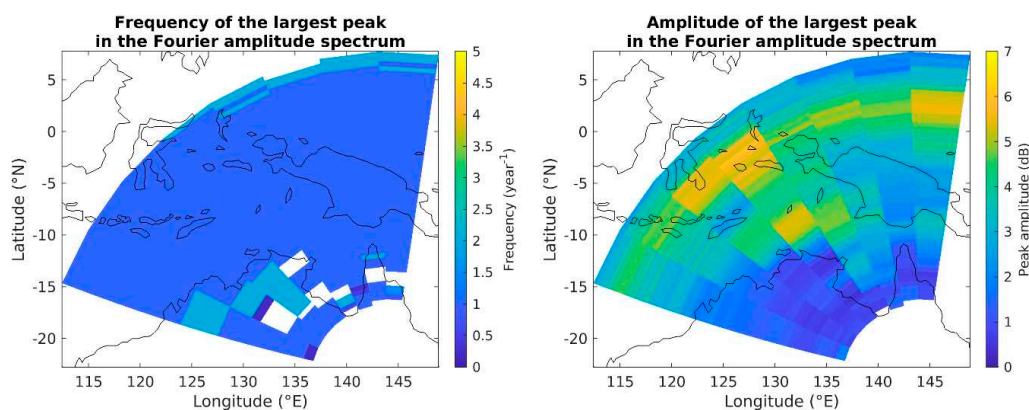


Figure 11. (Left): The frequency of the statistically significant (see text for details) primary peaks from the FFT for each LO range-azimuth cell. (Right): the amplitude of the largest peak from the FFT for each LO range-azimuth cell. Range-azimuth cells with greater than 50% missing data are excluded from the Fourier analysis.

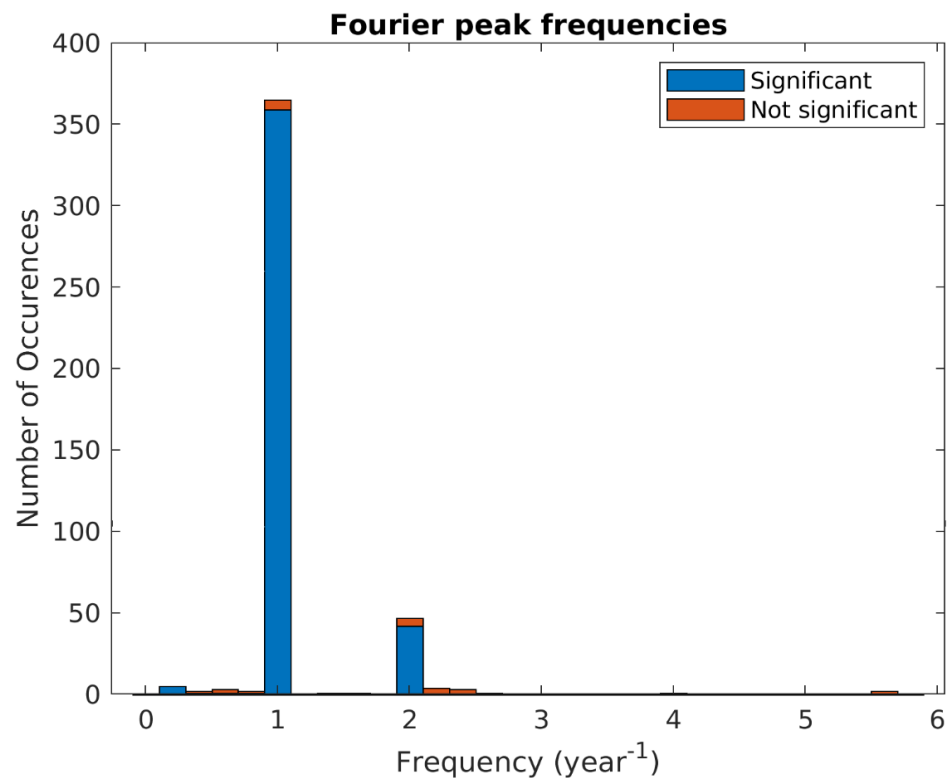


Figure 12. Histogram of the primary peak Fourier frequencies for the Longreach range-azimuth cells. Significant peaks are shown in blue, and peaks that are not significant are shown in red.

The frequency and amplitude of the second largest peak of the backscatter amplitude spectrum was also calculated in the manner described above for each range-azimuth cell of the LO data and plotted in Figure 13. Again, only the peaks considered statistically significant were included in the left most panel of Figure 13. The secondary-peak amplitude for all locations was low, especially in comparison with the amplitude of the primary peaks over the ocean. This indicates that most of the temporal variation in the backscatter coefficients occurs annually. A weak biannual variation is seen in the sea backscatter coefficients in certain regions.

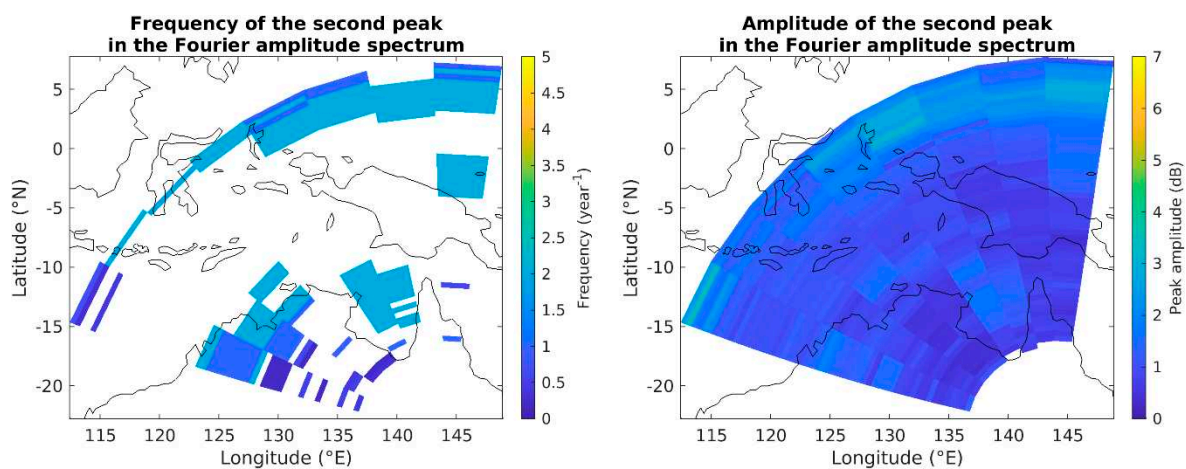


Figure 13. (Left): The frequency of the secondary peak from the FFT for each LO range-azimuth cell. (Right): the amplitude of the second largest peak from the FFT for each LO range-azimuth cell. Range-azimuth cells with greater than 50% missing data are excluded from the Fourier analysis.

Figure 14 shows a histogram of the secondary-peak frequencies for the LO range-azimuth cells. Many of the secondary peaks in the Fourier amplitude spectrum were not considered significant. The frequencies of the statistically significant secondary peaks were annual and biannual. Some of the spectral peaks at lower frequencies were also statistically significant. However, their amplitude was low and further it should be noted that these were generally for locations where a high percentage of data points were missing, and so these results should be treated with caution.

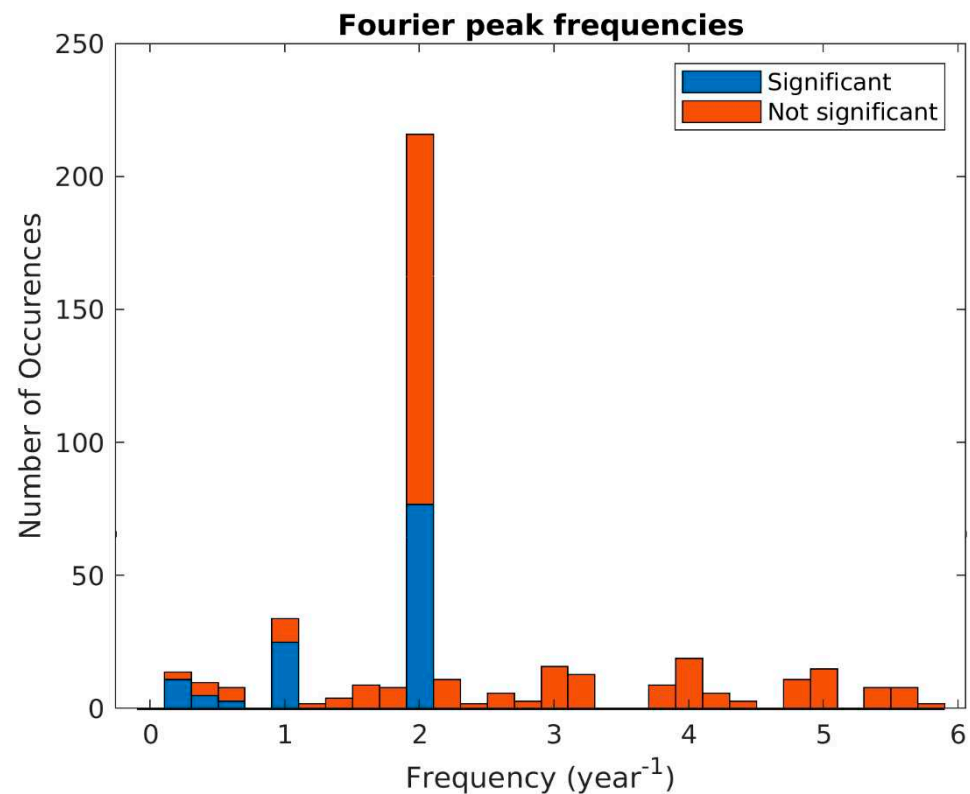


Figure 14. Histogram of the frequencies of the secondary peak in the Fourier amplitude spectrum for the Longreach range-azimuth cells.

Results from a Fourier analysis of data from each of the sounders are shown in Figure 15. The Fourier analysis for AS was done on a shorter nine-year data set, as no data was available before 2012. As with the Longreach sounder, the most common peak frequency in the Fourier spectra of the other sounders was also 1 year^{-1} . This peak was most prominent for the ocean around Indonesia (at 4°S , 125°E) and New Guinea (at 1°N , 145°E), which indicates that the largest seasonal variations in the sea surface backscatter coefficient occurs in these locations. Hemer et al. [27] show that for the Australian region the largest inter-annual variation in the significant wave height (normalized by the mean significant wave height) occurs around the location of these most prominent peaks: in the Gulf of Carpentaria (approximately 13°S , 139°E), the Arafura Sea (approximately 9°S , 136°E) and off the Queensland coast (approximately 15°S , 148°E). A yearly cycle in the surface backscatter coefficients over the land is also seen for many locations, although for this case the variation is weak as previously discussed. The biannual variation in the backscatter coefficient noted previously in Northern Australia (around 15°S , 135°E) in the LO data is also seen in the LAE results. Again, while statistically significant, this variation is weak as indicated by the peak frequency amplitude plots. The rainfall at the LAE BSS sites is low with little seasonal variation which peaks in November and so, as with the LO results, we cannot explain this biannual variation as being due to an instrumental effect caused by ground conductivity changes at the BSS transmit and receive sites.

Over the Australian land mass the amplitude of the peak frequency was low, indicating the seasonal change in the surface backscatter coefficients was small. Thus, for most applications a constant mean value for land locations will be sufficient to describe the backscatter coefficient. However, to describe the mean sea backscatter coefficient over time, monthly values must be used, noting this would not capture the day to day variations in the sea surface backscatter coefficients.

The phases associated with the annual and biannual variations in the backscatter coefficients are shown in Figure 16. In general the annual cycle (Figure 16 left) peaks around June to August for most ocean locations, which is expected [25]. Over the land the annual cycle tends to peak earlier in the year around March to May. This is around the end of the wet season in Northern Australia, when it is expected the ground would be at its wettest and hence have maximum conductivity.

The phase associated with the biannual cycle (Figure 16 right) is generally around 4 to 5 months, such that the backscatter coefficients peak around May/June and November/December each year. However, near the coast of Australia in the Indian Ocean (15°S , 117°E) around to the Timor Sea (11°S , 139°E) and also in the Gulf of Carpentaria (14°S , 139°E) the peak in the backscatter coefficient associated with the biannual cycle occurs around January and July each year.

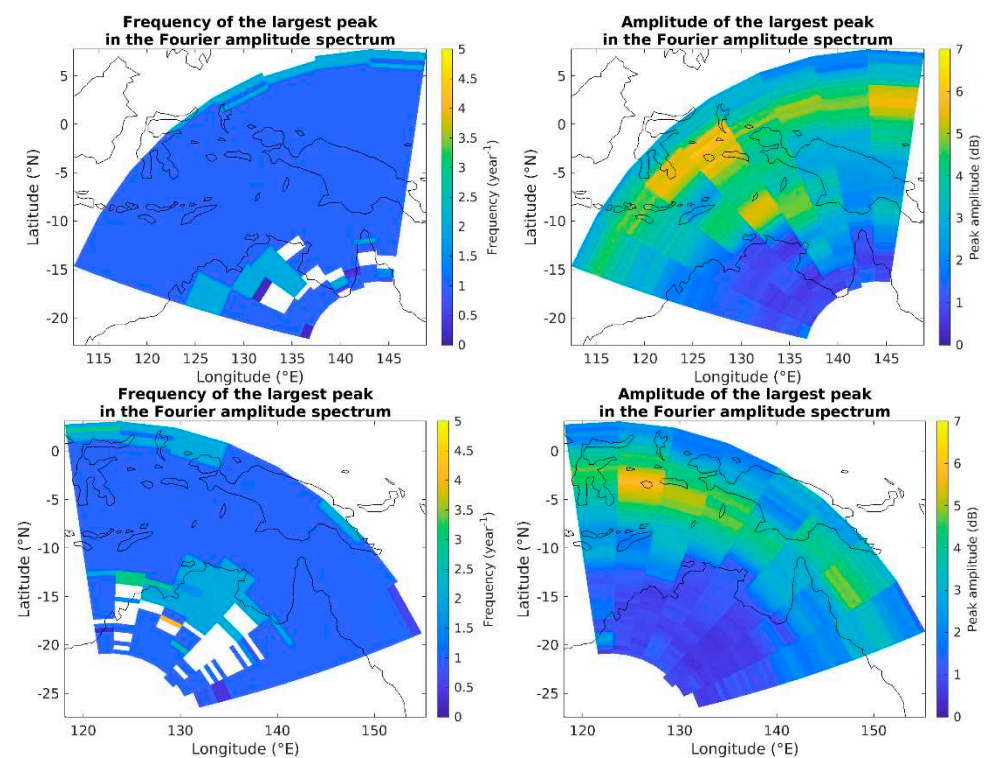


Figure 15. Cont.

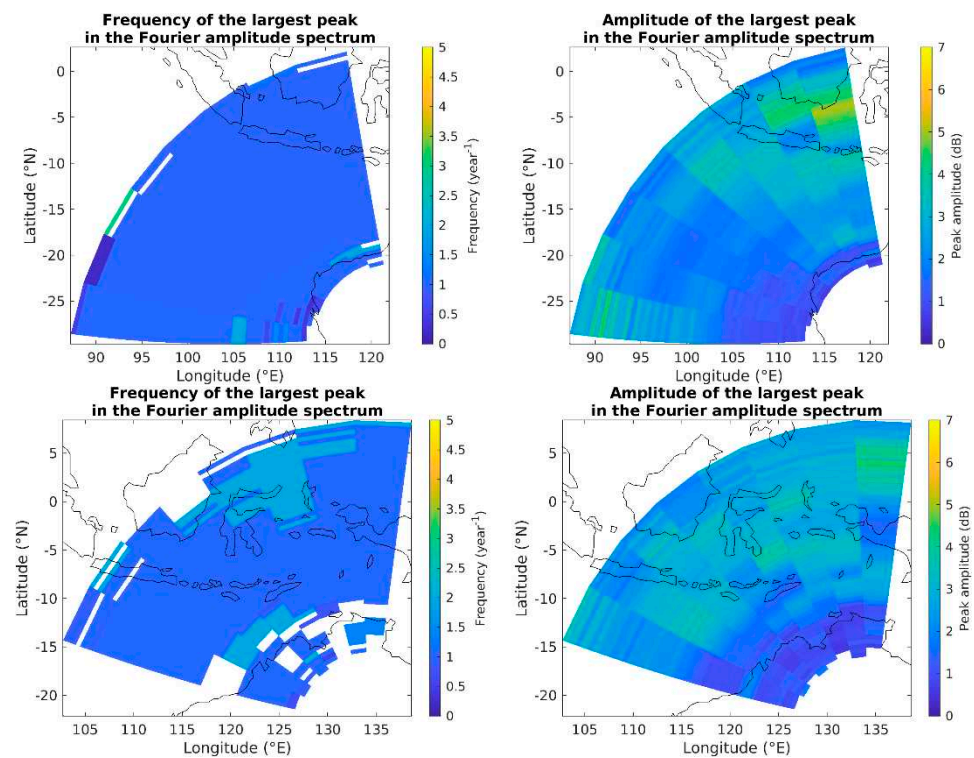


Figure 15. Fourier analysis on the LO, LAE, LAW and AS backscatter coefficients over a decade (listed from top to bottom). **(Left):** The frequency of the largest peak in the Fourier amplitude spectrum (only statistically significant peaks are shown). **(Right):** The amplitude of this largest peak.

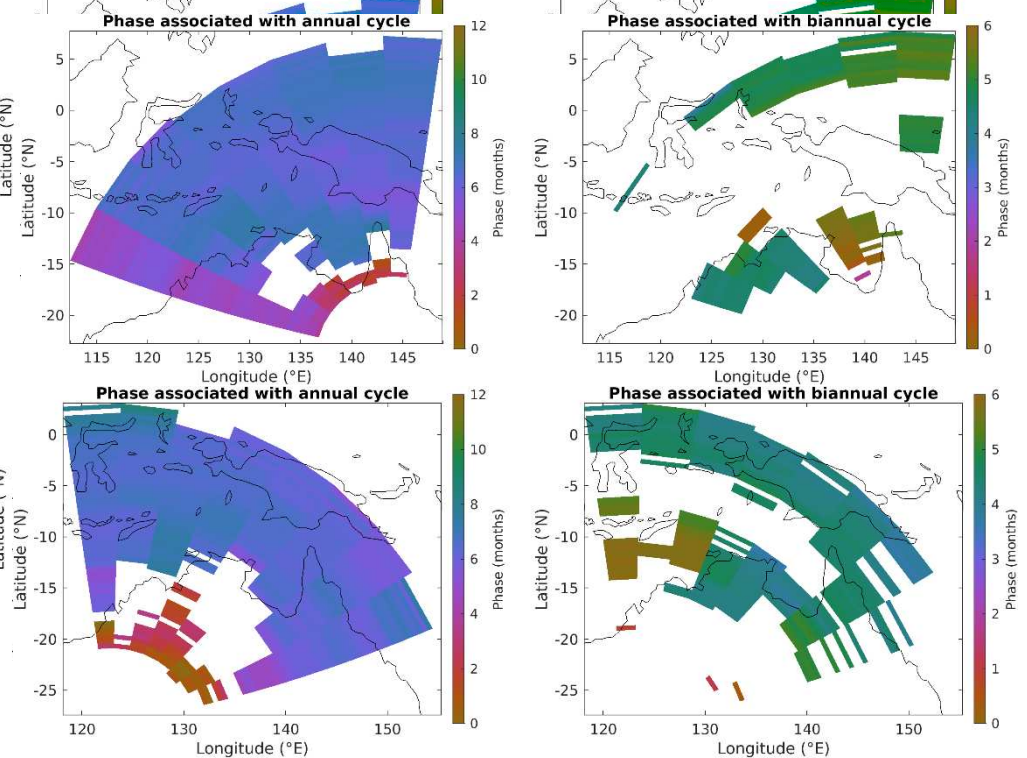


Figure 16. Cont.

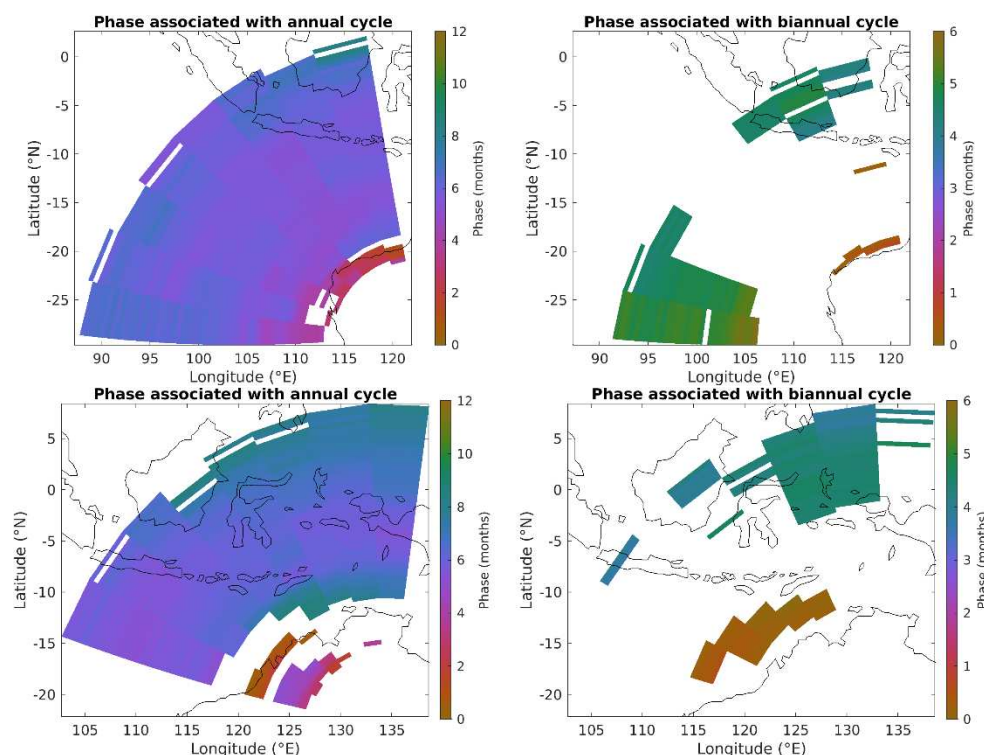


Figure 16. Phase from the Fourier analysis on the LO, LAE, LAW and AS backscatter coefficients (listed from top to bottom). **(Left):** The phase associated with the annual cycle. **(Right):** The phase associated with the biannual cycle. Phases of 0 and 12 months correspond to January. Only locations where a significant peak occurred at the specified frequency are shown.

3.3. Monthly Maps of the Surface Backscatter Coefficients

The analysis in the previous sections indicates that the variability in the sea backscatter coefficient is seasonal with little year-to-year variation and little variation at all for the land backscatter. Thus, we can construct monthly maps of the backscatter coefficient by combining the entire decade of data. We do this by calculating the decade mean of the monthly backscatter coefficients at each location.

The mean monthly backscatter coefficient maps for LO are shown in Figure 17. Changes in the backscatter coefficient throughout the year are clearly seen. The sea backscatter coefficients around Indonesia (at 4°S, 125°E) and New Guinea (at 5°S, 140°E) are significantly larger in the middle of the year, from around June to August, than at other times of the year. The backscatter coefficients over the Northern Australia landmass remained relatively constant throughout the year, with the lowest backscatter coefficients appearing over the Tanami desert (located around 20°S, 130°E).

Figures 18–20 show the mean monthly backscatter coefficients for LAE, LAW and AS. Similar trends to the LO results were found for these sounders, with larger sea backscatter coefficient generally seen in the middle of the year. In many areas the backscatter coefficients for the LAE sounder are significantly lower than the other sounders. This can be attributed to the field of view of LAE containing much of central Australia, which is predominantly desert and so has a lower backscatter coefficient. This is discussed in detail in our earlier paper [2].

The LAE observations also display an interesting and somewhat surprising feature with a strong seasonal variation in the backscatter coefficient from the island of New Guinea. The backscatter coefficient in central New Guinea is ~7dB stronger in August than in January. The single-sided amplitude spectrum from the FFT on the backscatter coefficient data from this location shows strong annual and biannual peaks (Figure 21). This behavior is in contrast to other land areas which show no seasonal variation in the backscatter coefficient. The strong backscatter from the inland region of this island is,

as discussed earlier, due to the large mountain range that runs along the length of the island. However, we have no explanation for the seasonal variation of the backscatter from this region. Indeed, we would expect any variation in the backscatter coefficient to be due to changes in the ground conductivity with a maximum during the rainy season. However, the rainy season in New Guinea occurs from December through to April when the backscatter coefficient is typically lower.

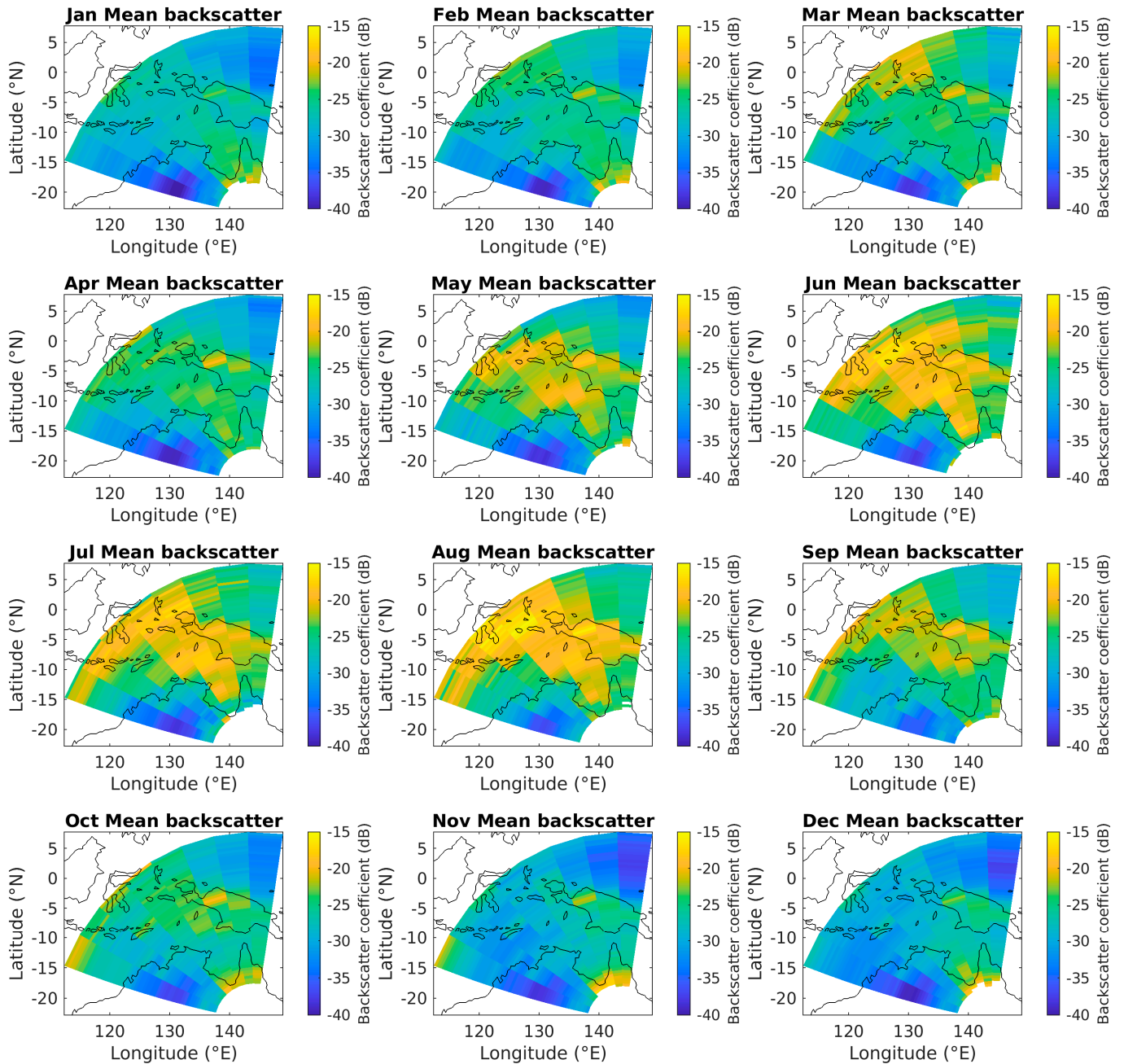


Figure 17. Decade mean of the monthly backscatter coefficients for LO.

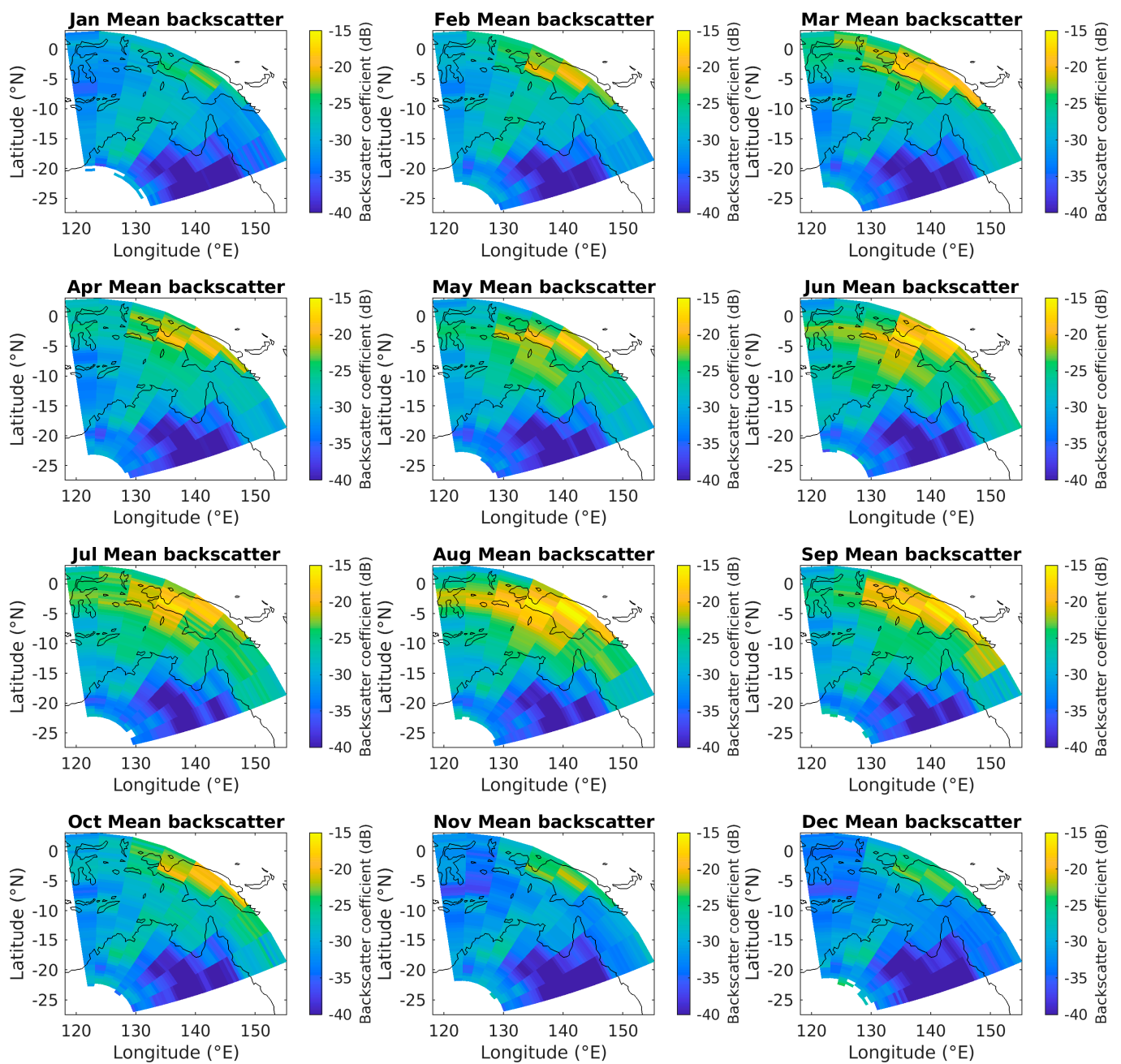


Figure 18. Decade mean of the monthly backscatter coefficients for LAE.

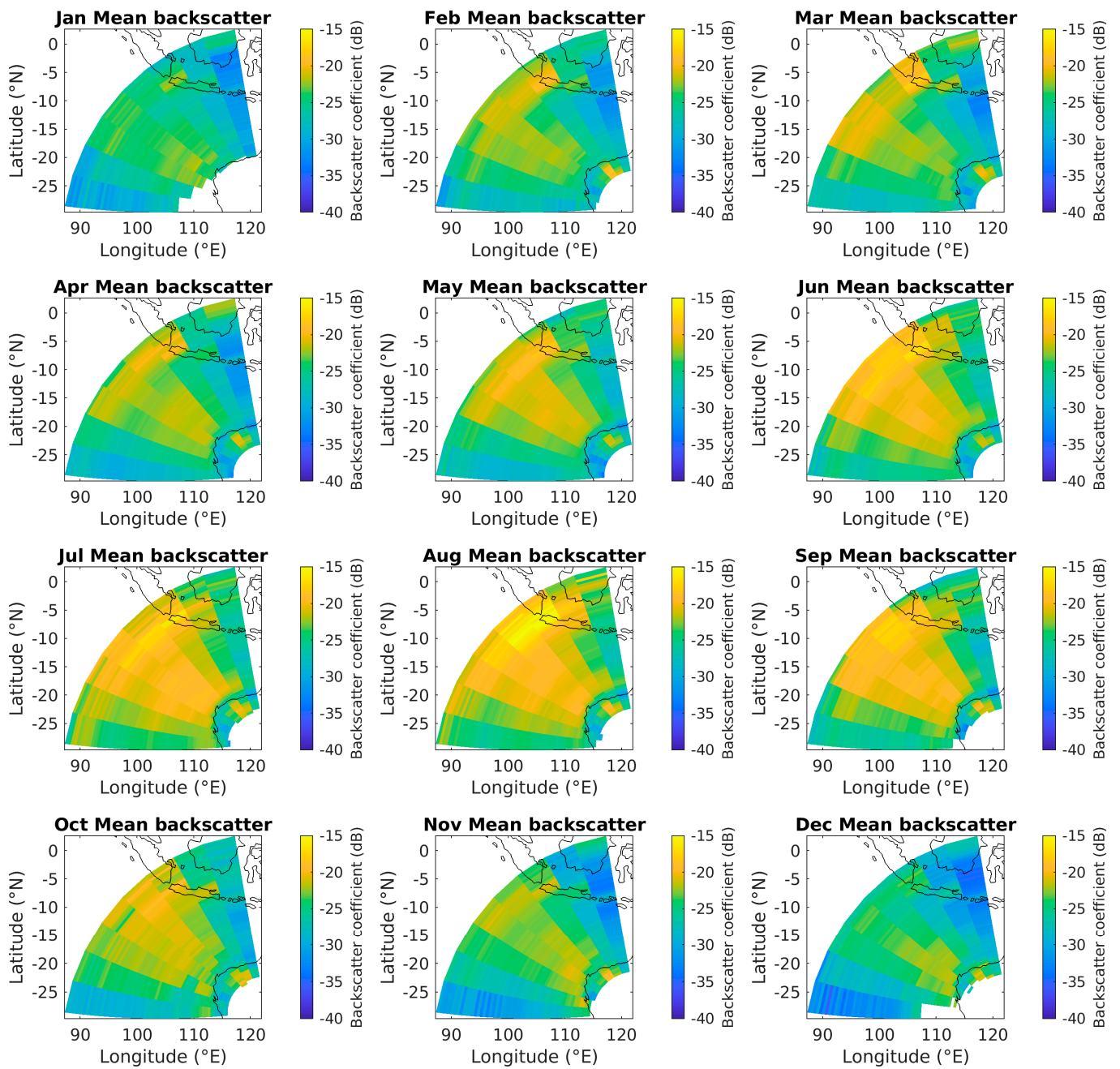


Figure 19. Decade mean of the monthly backscatter coefficients for LAW.

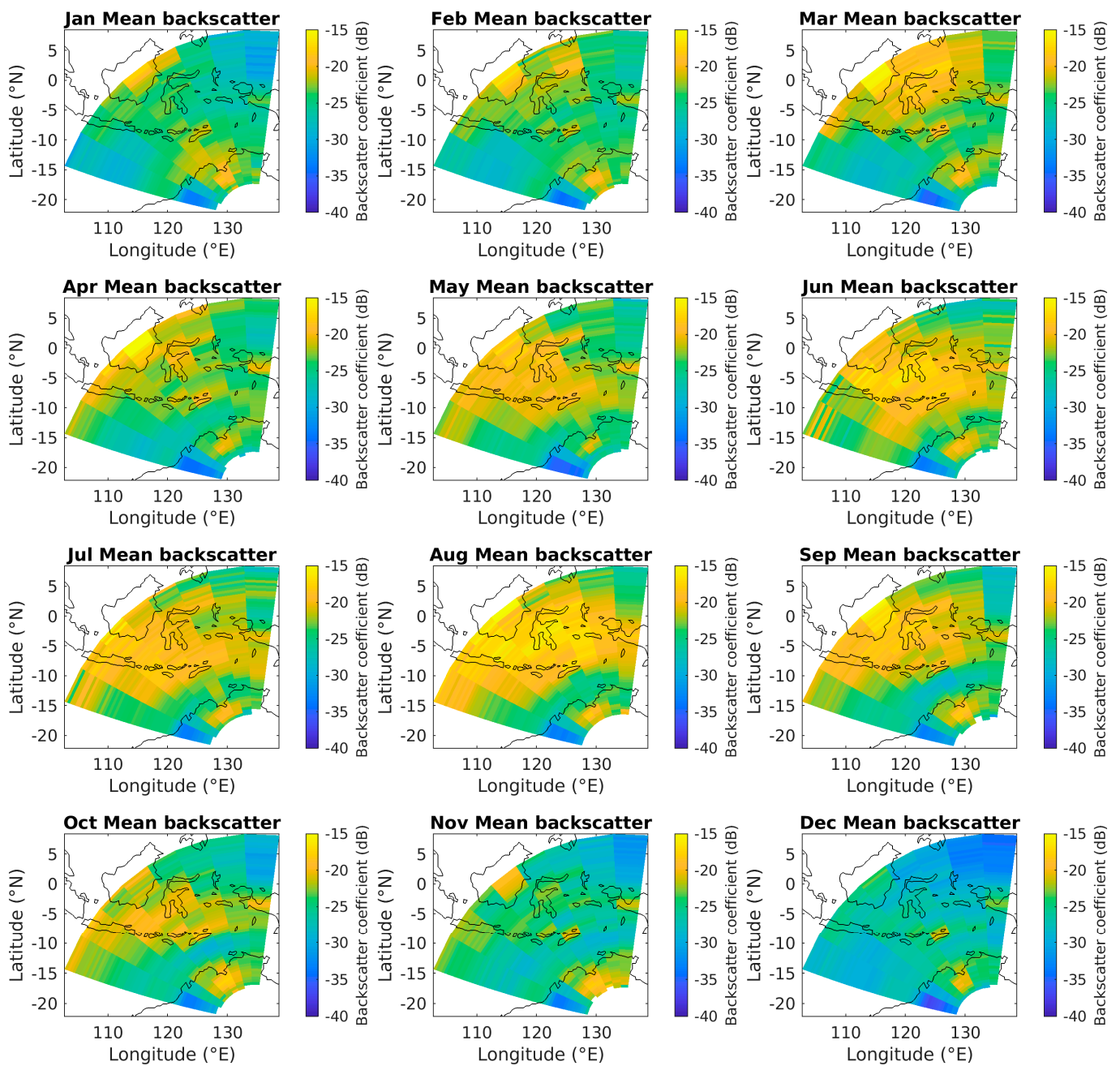


Figure 20. Decade mean of the monthly backscatter coefficients for AS.

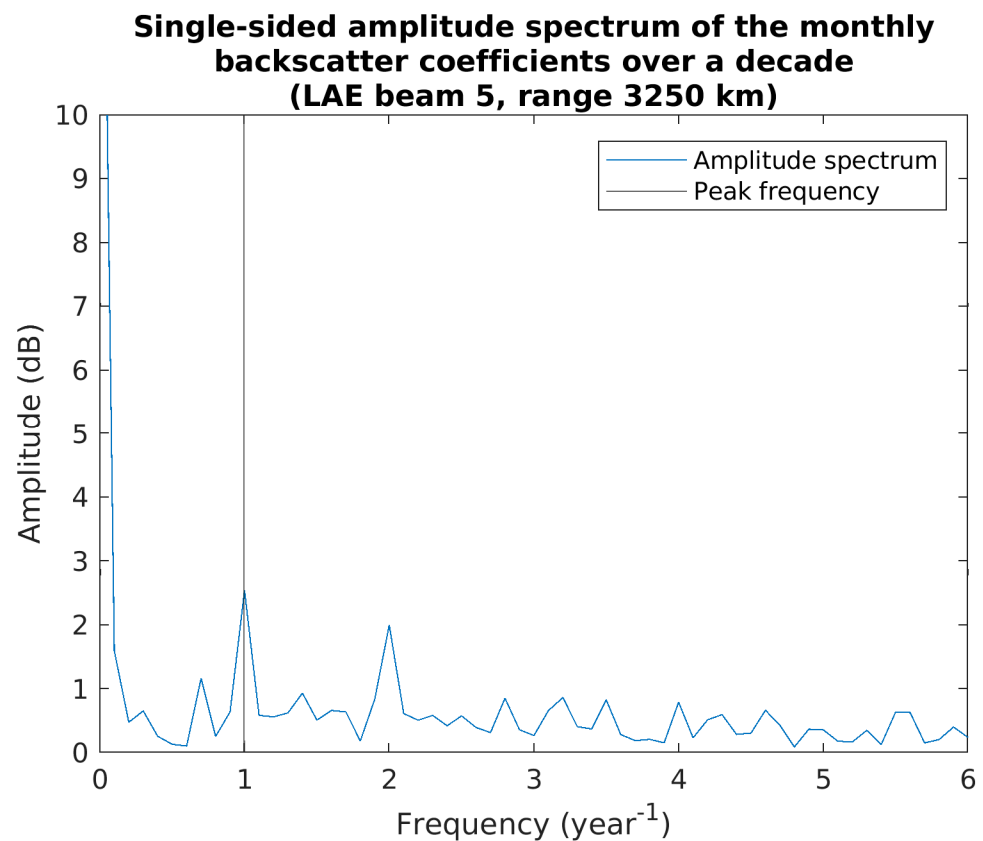


Figure 21. Single-sided amplitude spectrum from the FFT on the LAE beam 5, range 3250 km data.

The standard deviation between the months was also calculated. We have not included the plots here. However, the standard deviation of the land backscatter coefficients is less than 2 dB for most locations, while the standard deviation in the sea backscatter coefficients is larger, rising to 5–6 dB in some locations. This is in line with the Fourier analysis results discussed in the previous section and shows the sea backscatter varies considerably more throughout the year than the land backscatter. This is not surprising given the sea state is governed by the meteorological conditions. Hence, while the use of a single temporally invariant backscatter coefficient for land locations may be sufficient for many applications and locations, a seasonally varying backscatter coefficient is required for sea backscatter.

4. Conclusions

Backscatter coefficients were calculated over a decade, and these were found to be highly variable spatially and temporally. Monthly mean backscatter coefficients were used to investigate seasonal variations in the results.

Due to limitations of the method, variations on smaller time scales than a month were unable to be investigated. This was due to the limitations of modelling the ionograms, as discussed in [2]. However, the standard deviation in the monthly results does give an indication of the day to day variation in the backscatter coefficients. This showed that the day to day variations in the sea backscatter coefficients are significantly larger than the land backscatter coefficients.

A strong yearly cycle in the sea backscatter coefficients was found, with the standard deviation between months up to 6 dB. This was expected due to the impact of the meteorological conditions on the sea surface and hence the sea surface backscatter coefficient. Land backscatter coefficients remained relatively constant over the decade. This shows that changes in surface parameters such as the soil moisture due to rainfall had little impact on the surface backscatter coefficient.

These findings demonstrate that when using backscatter coefficients, for example to calculate the ionospheric propagation conditions for OTHR, a constant value over the Australian landmass may be suitable. However, when using sea surface backscatter coefficients one must understand that these are highly variable, both day to day and throughout the year. It should also be noted that the surface backscatter coefficients are aspect dependent and different values may be needed if a location is viewed from multiple directions.

Future research could involve using a higher azimuthal resolution data set of backscatter ionograms to create more detailed maps of the backscatter coefficient, in which specific surface features may be identified and investigated further. This high azimuthal resolution BSS data will be available after the JORN midlife upgrade known as Defence Project AIR2025 Phase 6 [19]. This could improve the utility of the surface backscatter coefficients for coordinate registration and could allow for the study of how various surface features change over time.

Author Contributions: Conceptualization, D.E. and M.C.; methodology, D.E. and M.C.; software, D.E. and M.C.; validation, D.E. and M.C.; formal analysis, D.E.; investigation, D.E.; resources, D.E. and M.C.; data curation, D.E.; writing—original draft preparation, D.E.; writing—review and editing, D.E. and M.C.; visualization, D.E.; supervision, M.C.; project administration, D.E. and M.C. All authors have read and agreed to the published version of the manuscript.

Funding: This research received no external funding.

Data Availability Statement: Backscatter sounder data and real-time ionospheric model data are owned by the Australian Commonwealth Government, Department of Defence. They may be made available on a case-by-case basis pursuant to Defence Science and Technology Group policy for public release of information by contacting the primary author.

Acknowledgments: The authors wish to acknowledge David Holdsworth and the staff of Defence Science and Technology Group, Australia for useful discussions and suggestions. Results were obtained using the HF propagation toolbox, PHaRLAP, developed by Defence Science and Technology Group, Australia. This toolbox is available from <https://www.dst.defence.gov.au/opportunity/pharlap-provision-high-frequency-raytracinglaboratory-propagation-studies> (accessed on 22 February 2021).

Conflicts of Interest: The authors declare no conflict of interest.

References

1. Norman, R.J.; Parkinson, M.L.; Dyson, P.L. Comparing HF radar backscatter from the Southern Ocean with ray-tracing results using the IRI model. In *Proceedings of the Workshop on the Applications of Radio Science, Hobart, Tasmania*; National Committee for Radio Science: Canberra, Australia, 2004.
2. Edwards, D.J.; Cervera, M.A.; MacKinnon, A.D. High Frequency Land Backscatter Coefficients over Northern Australia and the Effects of Various Surface Properties. *IEEE Trans. Antennas Propag.* **2022**, *70*, 5819–5830. [[CrossRef](#)]
3. Lipa, B.J.; Barrick, D.E. Extraction of sea state from HF radar sea echo: Mathematical theory and modeling. *Radio Sci.* **1986**, *21*, 81–100. [[CrossRef](#)]
4. Barrick, D.E.; Peake, W.H. A Review of Scattering From Surfaces with Different Roughness Scales. *Radio Sci.* **1968**, *3*, 865–868. [[CrossRef](#)]
5. Barrick, D.E. Grazing behavior of scatter and propagation above any rough surface. *IEEE Trans. Antennas Propag.* **1998**, *46*, 73–83. [[CrossRef](#)]
6. Althouse, E.L.; Davis, J.R. A Practical Evaluation of Earth-Backscatter Simulation and an Estimate of the HF Ground-Scatter Coefficient. *Radio Sci.* **1972**, *7*, 897–911. [[CrossRef](#)]
7. Steele, J.G. High-frequency backscatter from terrain with trees. *Proc. IEEE* **1967**, *55*, 1583–1590. [[CrossRef](#)]
8. Balsler, R.P.; Scott, T.D. Ground Backscatter Observed with High Resolution Oblique Sounders. *Radio Sci.* **1972**, *7*, 239–243. [[CrossRef](#)]
9. Barnum, J. High-frequency backscatter from terrain with cement-block walls. *IEEE Trans. Antennas Propag.* **1971**, *19*, 343–347. [[CrossRef](#)]
10. Holdsworth, D.A. Skywave over-the-horizon radar track registration using earth surface and infrastructure backscatter. In *Proceedings of the IEEE Radar Conference, Seattle, WA, USA, 8–12 May 2017*; pp. 0986–0991.
11. Barnum, J.R.; Simpson, E.E. Over-the-horizon radar target registration improvement by terrain feature localization. *Radio Sci.* **1998**, *33*, 1077–1093. [[CrossRef](#)]

12. Crombie, D.D.; Watts, J.M. Observations of coherent backscatter of 2–10 MHz radio surface waves from the sea. *Deep-Sea Res. Oceanogr. Abstr.* **1968**, *15*, 81–87. [[CrossRef](#)]
13. Barrick, D. First-order theory and analysis of MF/HF/VHF scatter from the sea. *IEEE Trans. Antennas Propag.* **1972**, *20*, 2–10. [[CrossRef](#)]
14. Yingwei, T.; Biyang, W.; Hao, Z.; Caijun, W.; Jing, Y.; Weimin, H. Wave Height Estimation from First-Order Backscatter of a Dual-Frequency High Frequency Radar. *Remote Sens.* **2017**, *9*, 1186. [[CrossRef](#)]
15. Edwards, D.; Cervera, M.; MacKinnon, A. A Comparison of the Barrick and Backscatter Ionogram Methods of Calculating Sea Surface Backscatter Coefficients. *Remote Sens.* **2022**, *14*, 2139. [[CrossRef](#)]
16. Oinats, A.V.; Nishitani, N.; Ponomarenko, P.; Ratovsky, K.G. Diurnal and seasonal behavior of the Hokkaido East SuperDARN ground backscatter: Simulation and observation. *Earth Planets Space* **2016**, *68*, 18. [[CrossRef](#)]
17. Gardiner-Garden, R.S.; Pincombe, A.H. *A Study of the Seasonal Pattern of Variability in the HF Radar Cross-Section of the Sea*; DSTO-DPP-0261; Intelligence, Surveillance and Space Division, DST Group: Edinburgh, Australia, 1996.
18. Cameron, A. The Jindalee operational radar network: Its architecture and surveillance capability. In Proceedings of the International Radar Conference, Alexandria, VA, USA, 8–11 May 1995; pp. 692–697.
19. Holdsworth, D.A.; Mulder, K.; Turley, M.D.E. Jindalee Operational Radar Network: New Growth from Old Roots. In Proceedings of the IEEE Radar Conference (RadarConf22), New York City, NY, USA, 21–25 March 2022; pp. 1–6.
20. Barnes, R.; Gardiner-Garden, R.; Harris, T. Real time ionospheric models for the Australian Defence Force. *Proc. WARS-2000* **2000**, *122135*, 122–135.
21. Harris, T.J.; Quinn, A.D.; Pederick, L.H. The DST group ionospheric sounder replacement for JORN. *Radio Sci.* **2016**, *51*, 563–572. [[CrossRef](#)]
22. Cervera, M.A.; Harris, T.J. Modeling ionospheric disturbance features in quasi-vertically incident ionograms using 3-D magnetoionic ray tracing and atmospheric gravity waves. *J. Geophys. Res. Space Phys.* **2014**, *119*, 431–440. [[CrossRef](#)]
23. George, P.L.; Bradley, P.A. A new method of predicting the ionospheric absorption of high frequency waves at oblique incidence. *Telecommun. J.* **1974**, *41*, 307–312.
24. Burke, G.; Poggio, A.; Logan, J.; Rockway, J. NEC—Numerical electromagnetics code for antennas and scattering. In Proceedings of the Antennas and Propagation Society International Symposium, Seattle, WA, USA, 18–22 June 1979; pp. 147–150.
25. Colosi, L.V.; Villas Bôas, A.B.; Gille, S.T. The Seasonal Cycle of Significant Wave Height in the Ocean: Local Versus Remote Forcing. *J. Geophys. Res. Ocean.* **2021**, *126*, e2021JC017198. [[CrossRef](#)]
26. Torrence, C.; Compo, G.P. A Practical Guide to Wavelet Analysis. *Bull. Am. Meteorol. Soc.* **1998**, *79*, 61–78. [[CrossRef](#)]
27. Hemer, M.; Church, J.; Hunter, J. Waves and Climate Change on the Australian Coast. *J. Coast. Res.* **2007**, *50*, 432–437.